Applied Energy 288 (2021) 116653

Contents lists available at ScienceDirect

Applied Energy

journal homepage: www.elsevier.com/locate/apenergy

Predictive energy management of residential buildings while self-reporting flexibility envelope

Jan Gasser [a], Hanmin Cai [a,*], Stavros Karagiannopoulos [b], Philipp Heer [a], Gabriela Hug [b]

[a] Urban Energy Systems Laboratory, Empa, Überland Str. 129, Dübendorf, Switzerland
[b] EEH - Power Systems Laboratory, ETH Zurich, Physikstrasse 3, 8092 Zurich, Switzerland

ARTICLE INFO

Keywords:
Flexibility envelope
Demand response
Model predictive control
Building energy management system
Self-report

ABSTRACT

In recent years, renewable energy resources have been increasingly embedded in the distribution grids, raising new issues such as reverse power flows, and challenging the traditional distribution system operation. In order to mitigate these issues, it has been proposed to operate the distribution system more flexibly. For instance, residential buildings are ideal candidates to offer energy flexibility locally and defer avoidable and expensive system expansions. Due to advances in smart meter technologies and trends towards digitalization, it becomes more and more common that electrical appliances in residential buildings are equipped with remote communication and control capabilities. This paper aims at quantifying a flexibility envelope of actively controlled flexible buildings and at analyzing the sensitivity of flexibility levels with respect to system configuration, control strategy and objective function settings. We consider rooftop photovoltaic units, air-sourced heat pumps for space heating and domestic hot water, thermal energy storage and electric vehicles. The results show that an optimal control aiming at minimizing energy costs while limiting peak power can lead to savings of up to 25% compared to the existing rule-based control. When carbon emissions are considered in the cost function, the optimized controller leads to an emission reduction of up to 21%. The time-dependent quantification of the flexibility envelope further reveals that high and low power levels can only be sustained for a limited period, whereas medium power levels can be sustained the longest.

1. Introduction

Recently, there have been growing incentives for increasing the penetration of distributed Renewable Energy Resources (RES) in the distribution system due to favorable policies, growing awareness on climate challenges, and promising economic assessments. While this supports the transition towards a more sustainable energy system, system operators cannot continue to operate their assets as in the past [1], when distribution grids were treated as sinks of power. Power quality issues such as reverse power flows are possible due to rooftop PV production at periods of high solar irradiance [2]. These reverse flows may reach levels at which expensive network expansion may become necessary based on traditional distribution system planning [3]. Simultaneously, the digitalization of electrical loads in residential buildings has also gained momentum, because of decreasing costs and increasing business potential linked to digitalization. Besides, the sizable storage in stationary batteries/EVs and high inertia of thermal systems enable building energy management systems to modify how buildings traditionally interact with the power system without compromising end-user comfort. Hence, there has been an increasing interest in combining these two trends and involve residential electrical appliances in the overall system management in a coordinated manner [4,5].

Although tapping buildings' flexibility presents an attractive alternative to traditional prohibitively expensive network expansions [2,6], these flexibility resources typically cannot be directly dispatched by system operators. Due to separate ownership of flexibility assets, system operators would have to estimate the flexibility measures of buildings and corresponding availability [7], or rely on buildings to regularly self-report to obtain a real-time overview of flexibility resources [8]. In addition, it is desired to have a generic flexibility quantification with as few metrics as possible, which would allow easier integration into existing system operation.

This study quantifies flexibility based on a flexibility envelope concept, which was initially proposed in [9]. The concept describes flexibility by a set of time indexes for which a constant power level can be sustained without loss of comfort. It provides a system operator with an overview of the total available flexible power levels and energy

* Corresponding author.
E-mail addresses: jan.gasser@alumni.ethz.ch (J. Gasser), Hanmin.Cai@empa.ch (H. Cai), karagiannopoulos@eeh.ee.ethz.ch (S. Karagiannopoulos), Philipp.Heer@empa.ch (P. Heer), hug@eeh.ee.ethz.ch (G. Hug).

https://doi.org/10.1016/j.apenergy.2021.116653
Received 23 November 2020; Received in revised form 8 February 2021; Accepted 11 February 2021
Available online 23 February 2021

Nomenclature

E	Energy [kWh]
J	Cost function [–]
P	Electric power [kW]
T	Temperature [°C]
ω	Weighting factor [–]

Abbreviation

COP	Coefficient of Performance
DHW	Domestic Hot Water
DHP	Domestic hot water Heat Pump
DR	Demand response
EV	Electric Vehicle
HP	Heat Pump
MPC	Model Predictive Control
PV	Photovoltaic
RES	Renewable Energy Resources
SHP	Space heating Heat Pump
SOC	State of Charge
TES	Thermal Energy Storage

Subscripts and superscripts

η	Efficiency [–]
t	Time step index
btg	Building to grid
gtb	Grid to building
a	Ambient
bat	Battery
cha	Charge
dis	Discharge
el	Electrical
f	Floor
fr	Floor to room
max	Maximum
min	Minimum
r	Room
ra	Room to ambient
rem	Remain
src	Source
snk	Sink
th	Thermal
wf	Wall to floor
wr	Return water

values. However, the concept is only investigated in a static setting and the flexibility of appliances operating on rule-based strategies is quantified in a retrospective analysis. The rule-based strategy limits appliances' capability of reacting to system-level signals, such as carbon intensity of electricity and electricity price. In addition, the authors of [9] do not elaborate on how the concept could fit into the overall real-time system operation, which is the focus of this paper. The current study first investigates energy scheduling and real-time flexibility quantification of electrical loads in a typical Swiss residential building. It is further highlighted that several factors have substantial impacts on the flexibility level, such as system configuration, control strategy, and objective function. Hence, a comparative analysis is further carried out in this study to evaluate the impact of these factors. The quantification of the flexibility at the building level is crucial for the understanding of the overall available level of flexibility. Although this study does not provide the means for an aggregated flexibility assessment of multiple households, we discuss the mechanisms qualitatively to integrate system-wide flexibility. The rest of this section provides a critical review of relevant literature.

The authors of [10] implement an economic MPC for a SH HP considering day-ahead electricity prices. Their results suggest that the MPC can effectively reduce energy costs. Ref. [11] applies MPC to optimize HP operation accounting for carbon intensity of electricity. However, it only investigates the flexibility due to building thermal inertia and does not consider other flexibility resources in the building. Although the results of both studies imply that flexibility is utilized in the MPC framework, the amount of flexibility is not quantified explicitly. Several means to calculate flexibility are investigated in [12], which proposes to standardize flexibility metrics so building flexibility can be integrated into a smart grid framework. However, the study is mainly a retrospective analysis with a specific focus on rebound effects. Flexibility factors of buildings operating on rule-based and predictive strategies are compared in [13]. Although flexibility is evaluated based on energy and power, it does not provide an estimation of the duration that a given power level can be sustained. Since flexibility is strongly dependent on initial conditions and time of the day, static energy and power flexibility quantification are not sufficient to represent the availability of flexibility. This availability is critical in real-time dispatch according to the large-scale pilot demonstration project EcoGrid 2.0 [14], in which a design of flexibility contracts for local flexibility markets is proposed. In such contracts, the duration of flexibility provision is explicitly defined as it is critical for service evaluation and calculating remuneration. An inner-box approximation approach is proposed in [15] to quantify aggregate power flexibility of distributed energy resources in an unbalanced distribution system. To simplify, the study considers only the power flexibility and assumes the flexibility is time-decoupled. The same approach is used in [16] to quantify the flexibility of behind-the-meter resources in one residential building. The study focuses on the coordination between a building energy management system and a Distribution System Operator (DSO). In their framework, a flexibility band is quantified and sent to the DSO, which returns a desired power profile to the building energy management system for implementation. In both studies, the flexibility is parameterized solely by electrical power without indicating how long a given power profile can be sustained. Ref. [17] represents flexibility with a cost curve. Multiple building energy optimization problems need to be solved to quantify incurred cost due to reference tracking and deviating from optimal plan. In addition, such calculations need to be repeated for each flexibility interval. The authors of [9] quantify the flexibility of smart electrical appliances in a large pilot experiment including washing machines, tumble dryers, dishwashers, DHW storage, and EVs. They first develop the energy flexibility envelope concept and their results show that flexibility has strong time dependency. However, none of these studies comprehensively quantifies the impacts of different system configurations, control strategies, and objective function settings.

This paper differentiates from the mentioned studies in terms of the main focus, quantification of flexibility, and system configuration. This is further summarized in Table 1.

The main contributions of this paper are summarized as follows:

1. The combination of a flexibility envelope concept and an MPC-based building energy management system to support real-time system-wide energy management.
2. A comparative analysis of the building energy flexibility with respect to the system configuration, control strategy, and objective function settings.
3. Real-time quantification of the flexibility envelope and self-report to system operators for system-wide dispatch.
4. The consideration of the carbon intensity of electricity at high temporal resolution.

Table 1
Comparison of relevant research works.

Ref.	Main focus	Flexibility quantification	EV/BESS	HP	TES
[9]	Flexibility quantification	Offline	✓	✓	✓
[10]	Bi-level economic MPC	–	✗	✓	✗
[11]	MPC & emission reduction	–	✗	✓	✗
[12]	Flexibility characterization	Offline	✗	✓	✓
[13]	Demand flexibility indicators	Offline	✗	✓	✓
[14]	Flexibility contract and market	Offline	✗	✓	✗
[15]	Transmission–distribution interaction	Online	✓	✓	✗
[16]	MPC & power flexibility band	Online	✓	✓	✗
[17]	Flexibility amount and cost	Online	✓	✓	✗
This paper	MPC & flexibility envelope	Online	✓	✓	✓

The remainder of the paper is organized as follow: Sections 2 and 3 provide models for electrical and thermal appliances, the control strategy description and a formulation for the flexibility envelope quantification. Section 4 presents simulation and comparative analysis results and a framework to incorporate flexibility into real-time operation. Finally, Section 5 gives a brief summary, and areas for further research are identified.

2. Mathematical models

This section summarizes the mathematical models of typical electrical and thermal components in Swiss residential buildings. In particular, EV, TES and HP have been identified as promising flexible resources because energy consumption in the building and transport sectors constitutes 65 % of total energy consumption in Switzerland [18]. Besides, HPs have been widely adopted since 2000 [19] because of their low environmental impacts and operating costs. During the same period, the registered EV numbers have increased from less than 1000 to more than 43 000 [20], accounting for 0.9% of all passenger cars. While HPs for DHW are generally equipped with water tanks as heat buffers, HPs for SH may or may not be complemented with a TES. Hence, both system configurations with and without TES are included in the comparative analysis. The rest of the section summarizes related models, whereas detailed parameters are presented in Section 4.

2.1. Thermal building model

To capture a building's thermal behavior, a resistance–capacitance model is used for its floor heating system. The model is adapted from [21] and [22]. It consists of three temperature states, namely the return water temperature T_{wr}, the floor temperature T_{f} and the room temperature T_{r}. The dependencies among the three states are given as follows:

$$\frac{\mathrm{d}}{\mathrm{d}t}T_{\mathrm{wr}} = \frac{1}{C_{\mathrm{wr}}}\left[P^{\mathrm{th}}_{\mathrm{src}} - K_{\mathrm{wf}}\,(T_{\mathrm{wr}} - T_{\mathrm{f}})\right], \tag{1a}$$

$$\frac{\mathrm{d}}{\mathrm{d}t}T_{\mathrm{f}} = \frac{1}{C_{\mathrm{f}}}\left[K_{\mathrm{wf}}\,(T_{\mathrm{wr}} - T_{\mathrm{f}}) - K_{\mathrm{fr}}\,(T_{\mathrm{f}} - T_{\mathrm{r}})\right], \tag{1b}$$

$$\frac{\mathrm{d}}{\mathrm{d}t}T_{\mathrm{r}} = \frac{1}{C_{\mathrm{r}}}\left[K_{\mathrm{fr}}\,(T_{\mathrm{f}} - T_{\mathrm{r}}) - K_{\mathrm{ra}}\,(T_{\mathrm{r}} - T_{\mathrm{a}}) + P^{\mathrm{th}}_{\mathrm{rem}}\right], \tag{1c}$$

where $P^{\mathrm{th}}_{\mathrm{src}}$ is the thermal power input into the heat distribution system from either the Space heating Heat Pump (SHP) or the TES, C_s ($s \in \{\mathrm{wr}, \mathrm{f}, \mathrm{r}\}$) are the heat capacities of the three temperature states and K_i ($i \in \{\mathrm{wf}, \mathrm{fr}, \mathrm{ra}\}$) are the heat transfer coefficients connecting the adjacent capacities. $P^{\mathrm{th}}_{\mathrm{rem}}$ represents the total heat demand of the Domestic hot water Heat Pump (DHP), the heat losses of the TES and the DHW storage, and T_{a} is the ambient air temperature. Internal gains and door and window openings are neglected in this study.

2.2. Heat pump model

The heat pump model is adopted from [23] and is given by:

$$P^{\mathrm{th}}_{\mathrm{HP}} = \mathrm{COP} \cdot P^{\mathrm{el}}_{\mathrm{HP}}, \tag{2a}$$

$$\mathrm{COP} = c_0 + c_1 T_{\mathrm{src}} + c_2 T_{\mathrm{snk}}, \tag{2b}$$

where T_{src} and T_{snk} are the temperatures of the heat source and the heat sink, respectively. The thermal power output P_{HP}th is expressed using the Coefficient of Performance (COP) and the electrical power input $P^{\mathrm{el}}_{\mathrm{HP}}$ to the HP. The COP is modeled as an affine function of the source and sink temperatures. In addition, the HP is assumed to be either switched off or operating at capacity, i.e. $P^{\mathrm{el}}_{\mathrm{HP}} \in \{0,\ P^{\mathrm{el,\ max}}_{\mathrm{HP}}\}$.

2.3. TES and DHW tank model

A TES is sometimes used as a heat buffer between the SHP and the heat distribution circuit of the SH to avoid frequent cycling of the SHP. The model of TES is adopted from [23] considering temperature rate of change, heat advection, diffusion and loss. This model captures adequately all relevant physical effects for the scope of this study and is given by:

$$\frac{\partial T}{\partial t} + v_{\mathrm{st}}\frac{\partial T}{\partial y} = a\frac{\partial^2 T}{\partial y^2} - k_{\mathrm{th}}(T - T_{\mathrm{r}}), \tag{3}$$

where a is the water thermal diffusivity, k_{th} represents the thermal heat loss coefficient, T_{r} is the ambient temperature of the storage, which is the room temperature in this study, and v_{st} is the advection velocity. Additional terms are included to capture the convection. The same model is used for the DHW storage tank.

2.4. Electric vehicle model

Certain types of EVs only allow unidirectional power flow, while others support bi-directional power flow and vehicle-to-grid capabilities. This work considers EVs of both types. The battery model is adopted from [24] and is given by:

$$\frac{\mathrm{d}}{\mathrm{d}t}E_{\mathrm{bat}} = \eta_{\mathrm{bat}}P_{\mathrm{cha}} - \frac{P_{\mathrm{dis}}}{\eta_{\mathrm{bat}}}, \tag{4}$$

where E_{bat} is the energy stored in the battery and $P_{\mathrm{cha}} \in \mathbb{R}_+$ and $P_{\mathrm{dis}} \in \mathbb{R}_+$ are the charging and discharging powers, respectively. The charging and discharging efficiencies are assumed to be equal and are represented by η_{bat}.

In addition, rooftop PV installation and uncontrollable loads are considered in the study. While the PV production is modeled according to solar irradiance, the aggregated uncontrollable load profile is obtained by scaling real measurements according to the number of residents. The PV model adopted from [25] and [26] is given in Appendix B. For the sake of conciseness, the discretization of the equations above is not detailed here and the interested reader is referred to [27] for more details.

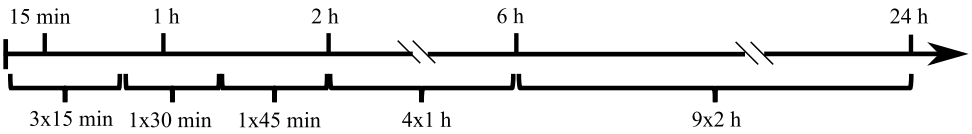

Fig. 1. Varying sizes of sampling time $\Delta\tau$ over an optimization horizon of 24 h.

3. Control strategy and flexibility envelope

3.1. Predictive control strategy

Existing residential building energy management systems commonly adopt rule-based control strategies, such as hysteresis control using on/off relays [28]. The relays switch on as soon as the storage is empty and switch off when it is full. This study focuses on an energy management system based on MPC, which is a rolling horizon optimization approach well suited to account for operational constraints, updating the forecast and system status amid uncertainties. Throughout the paper, an optimization horizon of 24 h is considered. To reduce the number of decision variables, multiple sampling time sizes are used over the optimization horizon, as shown in Fig. 1. The optimization time step is indexed as t, and the size of the corresponding sampling time is denoted as $\Delta\tau_t$.

The overall optimization problem can be formulated as follows:

$$\underset{x_t,u_t}{\text{minimize}} \sum_{t=1}^{N}\sum_{i=1}^{N_f} \omega_i J_i(x_t,u_t) + \sum_{t=1}^{N} R(x_t,u_t), \tag{5a}$$

$$\text{subject to } g(x_t,u_t) \le 0,\ \forall t \in \{1,\dots,N\}, \tag{5b}$$

$$h(x_t,u_t) = 0,\ \forall t \in \{1,\dots,N\}, \tag{5c}$$

$$x_t \in \mathbb{X},\ \forall t \in \{1,\dots,N\}, \tag{5d}$$

$$u_t \in \mathbb{U},\ \forall t \in \{1,\dots,N\}, \tag{5e}$$

where x_t denotes the state vector of building, thermal energy storage, water tank and EV, u_t denotes the electrical power of HP and EV, $\omega_i \in \mathbb{R}_+$ is the customized weighting factor associated with the ith sub-objective function $J_i(\cdot)$, N is the number of time steps over the optimization horizon shown in Fig. 1, N_f is the number of sub-objective functions, $R(\cdot)$ is the regulation term used to impose soft constraints on the states of some devices and penalize frequent cycling of HPs, $\mathbb{X}$ and $\mathbb{U}$ are the feasible space of the states and the inputs respectively. For simplicity, R_t is used below to denote $R(x_t,u_t)$. Constraints (5b) and (5c) include the devices models formulated in Eqs. (1) to (4) and the overall power balance. Constraints (5d) and (5e) are related to state and input power limits. Customized values are chosen for ω_i in the case studies. The rest of this section focuses on explaining different combinations of sub-objective functions $J_i(\cdot)$, which are motivated by practical needs.

3.1.1. Electricity cost minimization

Currently, Swiss households are billed with a two-tier electricity tariff. By combining anticipated price changes, user behavior and weather forecast, MPC controllers can optimize energy consumption to minimize energy cost. Minimizing the following objective function minimizes total energy cost and peak power penalty simultaneously:

$$\begin{aligned} J_{1,t} &:= (C_{\text{gtb},t} P_{\text{gtb},t} - C_{\text{btg}} P_{\text{btg},t})\Delta\tau_t, \\ J_2 &:= C_{\text{peak}} \times \max(\{|P_{\text{btg},t} + P_{\text{gtb},t}| \mid \forall t \in \{1,\dots,N\}\}), \\ &\text{minimize} \sum_{t=1}^{N} (\omega_1 J_{1,t} + R_t) + \omega_2 J_2, \end{aligned} \tag{6}$$

where ω_1 and ω_2 are the weighting factors used to balance between energy cost and peak power penalty, respectively, $P_{\text{gtb},t} \in \mathbb{R}_+$ and $P_{\text{btg},t} \in \mathbb{R}_+$ are the power flows from and to the grid respectively and only one of them can be non-zero at any time step, $C_{\text{gtb},t}$ refers to a local two-tier tariff [29], C_{btg} is a fixed feed-in-tariff for electricity injected into the grid and C_{peak} is a peak power penalty, and $\max(\{|P_{\text{btg},t} + P_{\text{gtb},t}| \mid \forall t \in \{1,\dots,N\}\})$ represents the peak power exchange with the grid within the optimization horizon.

3.1.2. Equivalent carbon emission minimization

The buildings themselves do not directly emit CO_2 since the considered system configuration does not include any fossil fuel-based appliances. Carbon emissions here refer to equivalent emissions considering the carbon footprint of the electricity taken from the grid. Although the main electricity generation in Switzerland comprises of hydro and nuclear power [18], the Swiss transmission network is also connected to neighboring countries allowing import and export of electricity. Depending on the generation sources of the electricity imported, the real-time carbon intensity of electricity can present high variances within the day and throughout the year. By shifting energy consumption outside the period of carbon-intensive generation, buildings contribute to reducing carbon emissions of the whole system. This paper considers only the carbon footprint of electricity taken from the grid and neglects carbon emissions associated with manufacturing and delivery of the appliances. Based on forecasts of the carbon intensity of electricity taken from the grid, the following objective minimizes the carbon emissions:

$$\begin{aligned} J_{3,t} &:= C_t P_{\text{gtb},t} \Delta\tau_t, \\ &\text{minimize} \sum_{t=1}^{N} (\omega_3 J_{3,t} + R_t), \end{aligned} \tag{7}$$

where ω_3 is the weighting factor with respect to carbon emissions, and C_t represents the time-varying carbon intensity of electricity imported from the grid. $P_{\text{btg},t}$ is considered emission free, but it does not offset the carbon footprint originating from net consumption.

3.1.3. Symmetric flexibility availability maximization

The availability of flexible power levels is dependent on the relative "distance" between devices' energetic status and their limits, which are imposed by comfort constraints, operational bounds and the available time to reach a specific status. For instance, if the State of Charge (SOC) of an EV's battery is significantly below the required level before an upcoming departure, high power levels might be needed to charge a vehicle. If time is a limiting factor, the lower the SOC is, the higher is the required power. If an EV has to be charged at its maximum power until departure to achieve the required SOC, the EV does not have any flexibility. Similarly, when the room temperature is close to its lower bound, a SHP needs to increase its power level to maintain thermal comfort, which also limits the possibility to keep the power at a low level. In these two scenarios, the availability of flexibility is asymmetric in the sense that available flexible power levels are only consumed or not, but not fed-back to the grid. Symmetric flexibility is more favorable since it can better serve future flexibility requests from the system operator.

With this notion in mind, we propose an empirical design of state trajectories that can be understood as the middle path which is equally distant from the upper and lower operational limits. By following these trajectories, there is equal space for both high and low power levels to be sustained. Based on this reasoning, the room temperature target

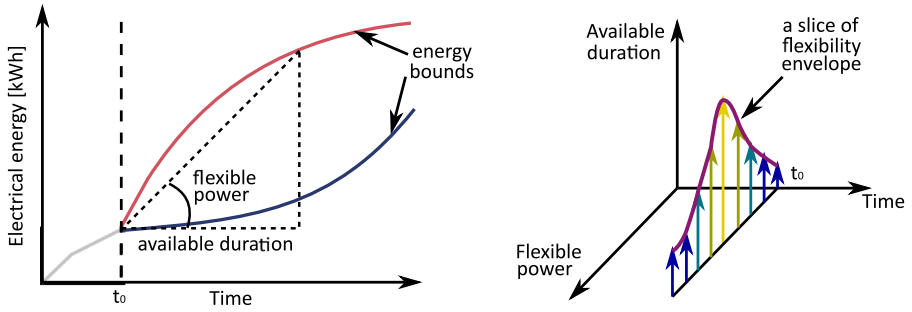

Fig. 2. Illustration of a flexibility envelope adapted from [9], where t_0 denotes next time step. Left figure depicts upper and lower energy bounds that allow derivation of flexible power and corresponding available duration. Right figure maps the time-varying power and duration into 3 dimensional space and the resultant purple curve represents a slice of flexibility envelope at t_0.

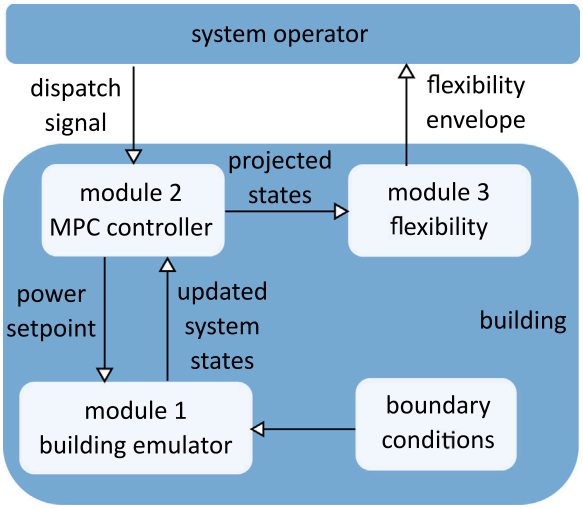

Fig. 3. Structure of overall simulation-based case study. Module 1 has a sampling time of 30 s whereas module 2 and 3 execute every 15 min. Interactions with system operator are not implemented and are depicted to illustrate the integration into system management.

trajectory is given by:

$$\begin{aligned} \Delta\tau^{\max} &:= \frac{T_{\mathrm{r}}^{\max} - T_{\mathrm{r},t}^{*}}{P_{\mathrm{SHP}}^{\max} - P_{\mathrm{loss},t}}, \\ \Delta\tau^{\min} &:= \frac{T_{\mathrm{r},t}^{*} - T_{\mathrm{r}}^{\min}}{P_{\mathrm{loss},t}}, \\ T_{\mathrm{r},t}^{*} &:= \frac{T_{\mathrm{r}}^{\min}(P_{\mathrm{SHP}}^{\max} - P_{\mathrm{loss},t}) + T_{\mathrm{r}}^{\max} P_{\mathrm{loss},t}}{P_{\mathrm{SHP}}^{\max}}, \end{aligned} \tag{8}$$

where $T_{\mathrm{r}}^{\max}$ and $T_{\mathrm{r}}^{\min}$ are the upper and lower room temperature limits, $P_{\mathrm{SHP}}^{\max}$ corresponds to the thermal power capacity of SHP, $T_{\mathrm{r},t}^{*}$ is the state on the target trajectory, and $P_{\mathrm{loss},t}$ is the average heat loss determined by the average ambient temperature forecast in the remaining horizon. $\Delta\tau^{\max}$ and $\Delta\tau^{\min}$ are defined as the duration that maximum and minimum power levels can be sustained before operational limits are reached. By setting $\Delta\tau^{\max} = \Delta\tau^{\min}$, we can obtain the state $T_{\mathrm{r},t}^{*}$ on the middle path.

Regarding EV, if the charging can be distributed evenly over the remaining time before departure, then there is no need for continuous high charging power right before being unplugged. The target energy storage trajectory of EV_j is given by:

$$\begin{aligned} P_{\mathrm{ev},j} &:= \frac{E_{\mathrm{ev},j,d} - E_{\mathrm{ev},j,0}}{\eta_{\mathrm{bat}} \Delta\tau_d}, \\ E_{\mathrm{ev},j,t}^{*} &:= E_{\mathrm{ev},j,0} + \eta_{\mathrm{bat}} P_{\mathrm{ev},j} \sum_{l=1}^{t} \Delta\tau_l, \end{aligned} \tag{9}$$

where $\Delta\tau_d$ is the remaining time until departure, $E_{\mathrm{ev},j,0}$ is the initial energy level, $E_{\mathrm{ev},j,d}$ corresponds to the required energy level at departure, and $E_{\mathrm{ev},j,t}^{*}$ represents the target energy trajectory of EV_j with the constant charging power $P_{\mathrm{ev},j}$.

Combining these two trajectories, the objective of maximizing symmetric flexibility availability is given by:

$$\begin{aligned} J_{4,t} &:= (C_{\mathrm{gtb},t} P_{\mathrm{gtb},t} - C_{\mathrm{btg}} P_{\mathrm{btg},t}) \Delta\tau_t, \\ J_5 &:= C_{\mathrm{peak}} \times \max(\{|P_{\mathrm{btg},t} + P_{\mathrm{gtb},t}| \mid \forall t \in \{1, \dots, N\}\}), \\ J_{6,t} &:= (T_{\mathrm{r},t}^{*} - T_{\mathrm{r},t})^2 \Delta\tau_t, \\ J_{7,t} &:= \sum_{j=1}^{N_{\mathrm{ev}}} (E_{\mathrm{ev},j,t} - E_{\mathrm{ev},j,t}^{*})^2 \Delta\tau_t, \\ \text{minimize} & \sum_{t=1}^{N} (\omega_4 J_{4,t} + \omega_6 J_{6,t} + \omega_7 J_{7,t} + R_t) + \omega_5 J_5, \end{aligned} \tag{10}$$

where ω_4 and ω_5 are the weighting factors penalizing energy costs and peak power, respectively, N_{ev} is the number of EVs, and $E_{\mathrm{ev},j,t}$ is the EV_j's energy level at time t. Deviations of room temperature and EV energy level from the target trajectories are penalized by the weighting factors ω_6 and ω_7 respectively.

3.2. Flexibility envelope

The flexibility envelope calculation starts with identifying energy bounds. When setting all devices to consume as early and as much as possible, the devices will first operate at maximum power and then reduce their power levels because they approach their operational limits, e.g. thermal constraints of TES fall into this category. Thus the electrical energy consumption increases monotonically with a steep slope at the beginning as the red curve shows in Fig. 2. Similarly, by setting all the devices to consume as late and as little as possible, the devices will first operate at minimum power and then increase their power levels because they approach their operational limits. This allows us to obtain the lower energy bound shown as the blue curve in Fig. 2. The region between these two curves defines all the feasible power levels of one building. Essentially, this flexibility region is determined by system dynamics and boundary conditions. Any line segment starting from current energy state and falling inside the region represents a flexible power level. The slope of the line segment defines the power while the second endpoint defines the available duration of such power level $P \in \mathbb{R}_+$. Denote time after t_0 as $\tau \in \mathbb{T}_+$, the sustained duration of different power levels can be expressed as $f : \mathbb{R}_+ \times \mathbb{T}_+ \to \mathbb{R}_+$. The flexibility envelope is essentially a three dimensional surface spanned by time, flexible power and available duration, with all the points defined by the set $\{(P, \tau, f(P,\tau)) | \tau \in \mathbb{T}_+, P \in \mathbb{P}_\tau\}$, in which $\mathbb{P}_\tau$ is the set of all flexible power levels at τ. Availability of high power level is limited by the upper energy bound, whereas the availability of low power level is limited by the lower energy bound.

To calculate control outputs and flexibility envelopes three modules are defined as illustrated in Fig. 3. Module 1 emulates detailed device

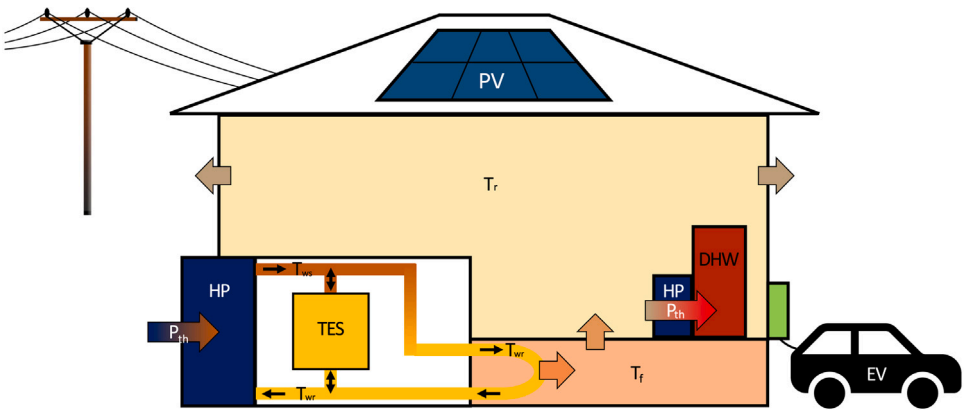

Fig. 4. A schematic overview of a multi-family building in Switzerland. The investigated building is equipped with a PV, a TES, HPs for DHW and SH, and two EVs.

Table 2
Room temperature set-point and temperature bounds.

Parameter	Value [°C]	Parameter	Value [°C]
T_r^{min}	21.5	T_r^{max}	22.5
T_{TES}^{min}	28.0	T_{TES}^{max}	42.0
T_{DHW}^{min}	41.0	T_{DHW}^{max}	59.0

dynamics with a sampling time of 30 s. Module 2 implements the control strategies formulated in Section 3.1. In the case of predictive strategies, the optimization is executed every 15 min, which provides projected state trajectories for the next 24 h. Module 3 further uses projected states as initial conditions to calculate the flexibility envelope, while taking into account anticipated boundary conditions. Note that when distribution system operational limits are considered, the flexibility region of the building energy management system may be reduced to avoid the risk of concurrent peak power. This is reflected in the communication of a dispatch signal and the flexibility envelope depicted in Fig. 3. The building that reacts to such dispatch signal is said to be network-aware in the sense that the dispatch signal originates from network health assessment.

4. Case study

A well-insulated multi-family building with nine residents is considered in the case study. A schematic overview of the electrical and thermal system configuration is shown in Fig. 4. The system includes rooftop PV installations, air sourced HPs for SH and DHW, a TES and two EVs. Both configurations with and without TES are studied to identify the impacts of TES on flexibility levels. The mixed-integer linear problem is formulated using YALMIP [30] in MATLAB and solved with Gurobi [31].

4.1. Input data and assumptions

The DHP electrical power capacity is P_{DHP}^{max}= 1.0 kW. The DHW tank volume is set to be 0.5 m^3, which corresponds to approximately 50 liters of storage volume per resident. SHPs with an electrical power capacity of P_{SHP}^{max}= 3.6 kW and P_{SHP}^{max}= 4.4 kW are used for systems without and with TES, respectively. When a TES is considered, a volume of 2 m^3 is assumed. The thermal comfort zones are listed in Table 2, with a room temperature set-point assumed to be 22 °C. As for the EVs, the minimum SOC at departure is set to 0.8. Table 3 lists key parameters of the two EVs. Typical weekly driving profiles are given in Tables 5 and 6 in Appendix A. Both EVs are assumed to charge at home only.

The boundary conditions are based on historical data obtained from [32,33] and [34]. The weekly profile of two-tier electricity tariff, a fixed feed-in-tariff of 0.05 CHF/kWh, as well as the monthly peak power penalty of 11.95 CHF/kW are taken from a local DSO [29]. In this paper, only HPs and EV charging stations are actively controlled. Other appliances such as dishwashers are left uncontrolled. Nonetheless, the aggregated profile of uncontrolled loads is included in the analysis when we calculate energy cost, emissions and peak power in Section 4.2. All input profiles for a week in spring are shown in Fig. 5. In all predictive controllers, perfect forecast and knowledge of the boundary conditions are assumed. Interested readers are referred to [27] for analyses of other seasonal conditions.

4.2. Controller performance comparison

One rule-based controller and three MPC controllers with different objective functions have been implemented in this study. All controllers are evaluated for ten days. In particular, all MPC-based controllers are required to have the same SOC as the rule-based controller for all storage devices at the end of the ten-day period in order to ensure a fair comparison. Figs. 6 and 7 compare all four controllers with respect to three metrics: energy cost, Green House Gas (GHG) emissions, and self-sufficiency. Self-sufficiency represents building's capability to cover its electricity need without importing from the grid. It is defined as:

$$S = \frac{E_{tot} - E_{gtb}}{E_{tot}} \tag{11}$$

where E_{tot} is the total electricity consumption and E_{gtb} is the total electricity imported from the grid.

Results show that the cost-oriented controller achieves the best performance in cost reduction and self-sufficiency improvement. A cost reduction of 22 % and self-sufficiency improvement of 58 % can be observed in Fig. 6. While the emission-oriented controller reduces emission and improves self-sufficiency, the resultant energy cost is higher than the rule-based controller. The flexibility-oriented controller achieves energy cost reduction and marginal improvement in self-sufficiency, but its equivalent emission is higher than the rule-based controller.

It can be observed that the TES can often achieve a higher relative cost saving compared to the rule-based strategy when comparing Fig. 6 with Fig. 7. However, comparing the absolute numbers shows that the MPC controllers provide a similar performance regardless of TES's existence. In addition, the rule-based controller performs worse with a TES than without a TES, because including a TES in the thermal distribution circuit requires a higher supply water temperature, which induces a lower COP. Hence, the lower COP of the SHP leads to a higher electricity consumption given the same thermal demand. The results also show that the use of a TES does not bring any advantage regarding energy costs or carbon emissions reduction.

When maximizing flexibility availability, the carbon emission reduction and self-sufficiency objectives are compromised and, as expected,

Table 3
Parameters of the two EVs considered in the study.

	E_{ev}^{max} [kWh]	P_{cha}^{max} [kW]	P_{dis}^{max} [kW]	ΔE [kWh/100 km]	Bidirectional charging
EV_1	53	11	0	19.5	✗
EV_2	40	7	7	22.1	✓

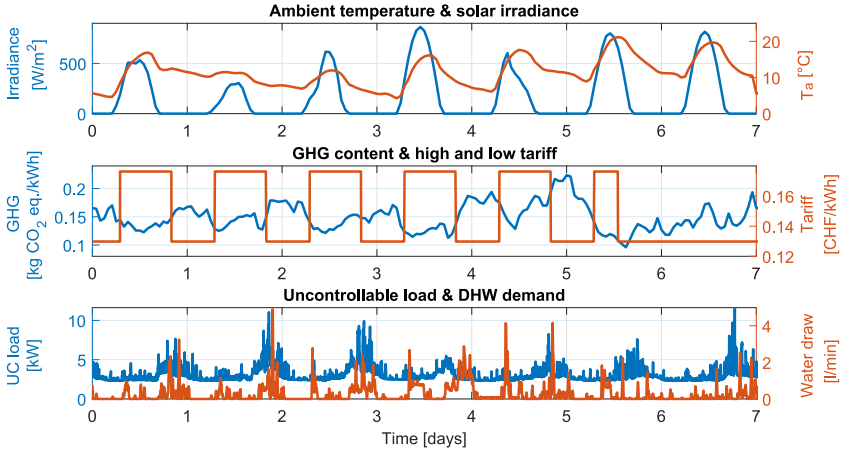

Fig. 5. Weekly profiles of ambient temperature (T_a), solar irradiance, carbon intensity of electricity from grid (GHG), two-tier electricity tariffs, aggregated electricity consumption of uncontrolled loads (UC load) and hot water draw. All the weekly profiles start on Monday morning and end on Sunday night.

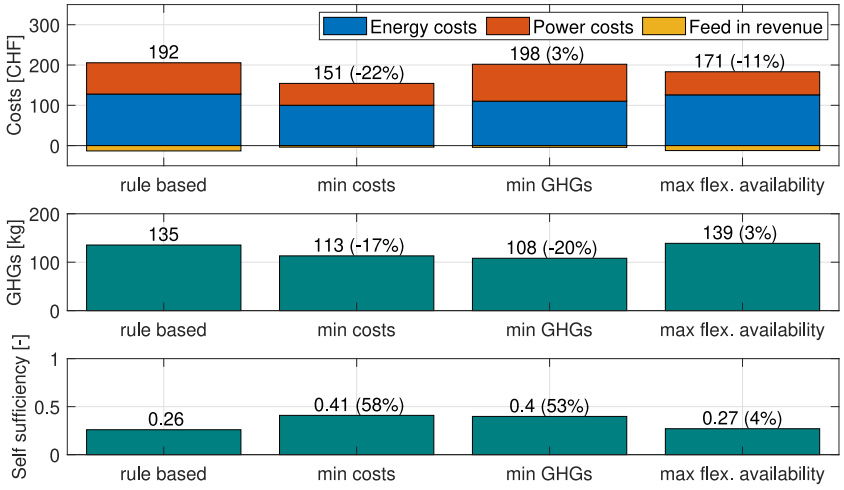

Fig. 6. Comparison of four different controllers for the system configuration without TES. Absolute values are specified for all the metrics, while relative changes in percentage compared with rule-based benchmark are presented in the brackets.

the pure cost-oriented controller achieves the highest cost saving in all cases. All MPC-based schemes increase the building's energy self-sufficiency, especially with cost-oriented and emission-oriented controllers. There are mainly two reasons. Firstly, it is more economical to use onsite PV production than to sell it to the grid and buy it back later because the feed-in-tariff is much lower than the two-tier electricity tariff. Secondly, since local PV production is considered free of emission, minimizing carbon emission simultaneously maximizes building energy self-sufficiency. These analyses are further visualized in Table 4. Note that perfect forecasts are assumed in all the predictive controllers. Hence, the results shown in Figs. 6 and 7 are the theoretically best achievable results. In practice, forecasts are associated with sizable errors, and achievable benefits will be lower than shown. Moreover, the numerical values will also vary with a different set of weighting factors.

Cost savings of 16 % and emission savings of 10 % are achieved in the winter case. However, the most interesting results are achieved in the summer case, where 26 % of costs are saved and emissions are reduced by 29 %. In the autumn case, the performance of the different controllers is similar to that in the spring case. The interested reader is referred to [27] for more details.

Table 4
Comparative analysis of MPCs with different objective functions. ✓ means TES is considered, while ✗ means TES is not included. + denotes improved performance in comparison with the rule-based benchmark, while - denotes decreased performance. In both cases, the number of the symbols visualizes the improved/decreased performance.

Objective function	TES presence	Cost saving	GHG reduction	Self-sufficiency
min costs	✗	++++	++	++++
	✓	++++	+	++++
min GHGs	✗	–	+++	+++
	✓	+	++++	++++
max flex. availability	✗	+++	–	+
	✓	++	––	+

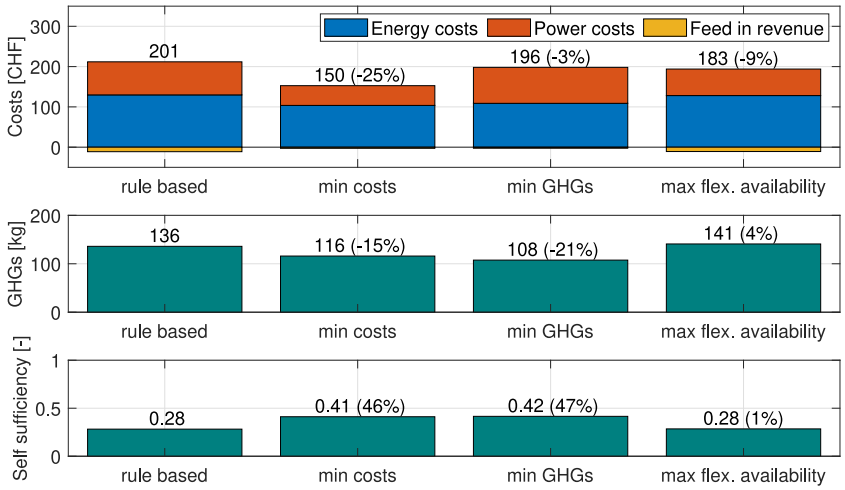

Fig. 7. Comparison of four different controllers for the system configuration with a TES of 2 m^3. Absolute values are specified for all the metrics, while relative changes in percentage compared with rule-based benchmark are presented in the brackets.

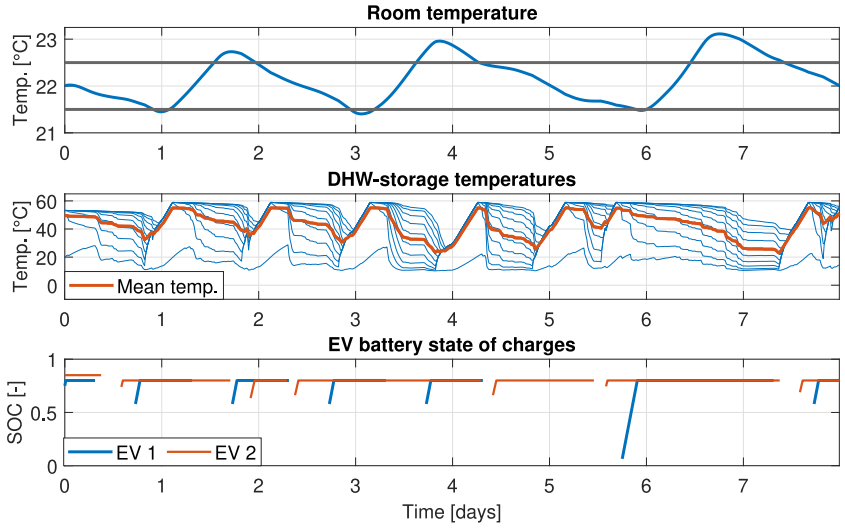

Fig. 8. System states based on rule-based control without TES. The middle sub-figure shows the average temperature of the DHW tank in red, and temperature of each layer in blue.

4.3. Flexibility envelope quantification

The state profiles given in Figs. 8, 10, 12, 14 and 16 are used as initial conditions to compute the various power levels and their availability as shown in Figs. 9, 11, 13, 15 and 17. In all cases, maximum available flexibility duration is limited to 48 h. In practice, a longer duration does not necessarily provide more information due to forecast errors.

4.3.1. Results for rule-based controller

The system states evolution over time in the rule-based case is summarized in Fig. 8. It can be observed that temperatures temporarily leave the predefined tolerance band due to the large thermal inertia of the system and high ambient temperature. An example is the overshoot on day 7. The DHW tank is discretized into ten layers. Fresh water enters the storage tank at the bottom layer and heating power is input via the layer above. Hot water is drawn from the top layer. Heat loss and DHW usage result in decreasing temperatures over time. Finally, the bottom figure illustrates the SOC of both EVs. The rule-based controller charges the batteries at full power as soon as an EV is connected to the charging station.

Fig. 9 displays the different constant power levels, including the maximal duration of all flexible devices. We observe that low power levels can sustain the longest (shown in yellow). The blue color for high power levels indicates availability for only a shorter duration and this is due to storage capacity limitations and comfort constraints. The availability of power levels is strongly dependent on available devices. Notably, most high power levels are only available when the EVs are connected. The variation of the yellow band can be explained by the fluctuation of the ambient temperature and the room temperature subsequently. If the room temperature is close to the upper bound, the SHP can operate at full power for a short period. But it can remain off for a long time and vice versa.

4.3.2. Results for cost-oriented MPC controller

The cost-oriented controller makes use of the room temperature tolerance band to minimize energy costs according to Fig. 10. This leads to the observed oscillation of the yellow band. The cost-oriented MPC controller sometimes charges EVs late. Hence, EVs are not flexible in these moments and have to be charged with high power in order to achieve the desired SOC at departure. Consequently, the yellow band in Fig. 11 indicating power levels that can be sustained for a long period is interrupted. This also illustrates the notion of biased flexibility availability in Section 3.1.3.

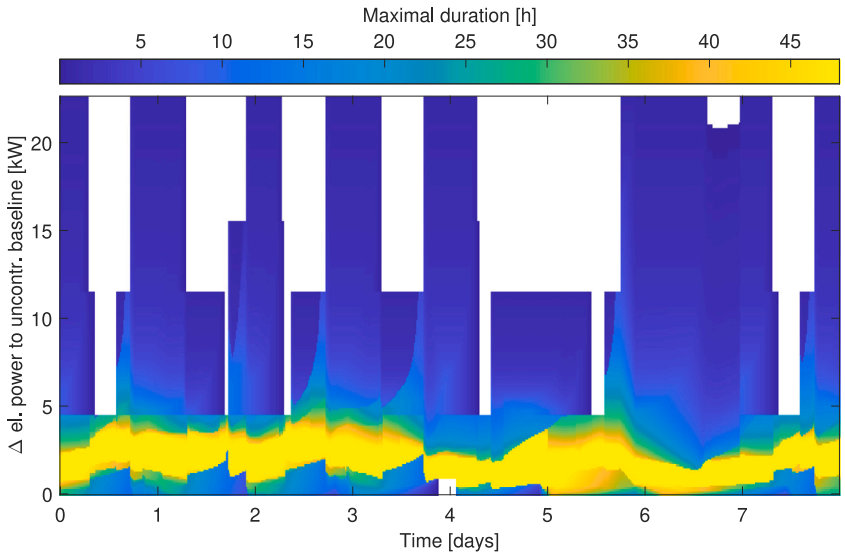

Fig. 9. Flexibility envelope of a building operated by a rule-based controller without TES. The white area indicates infeasible power levels at the specific times.

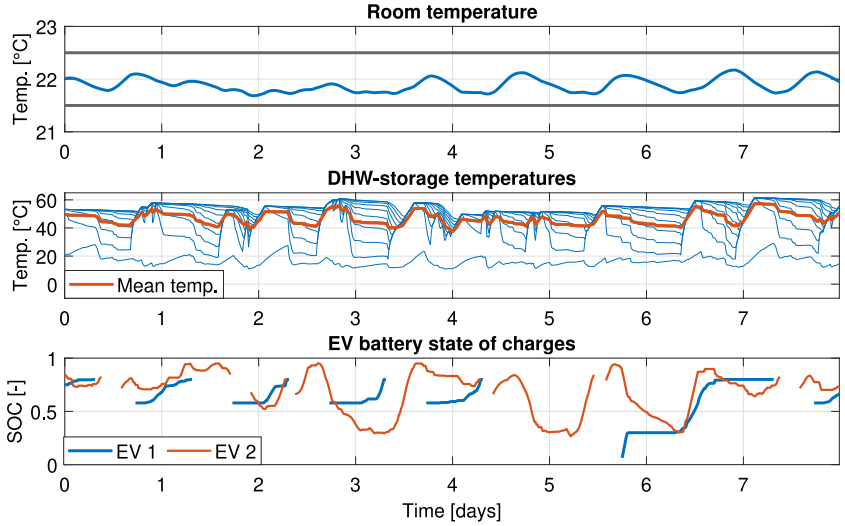

Fig. 10. States of the building without TES operated by a cost-oriented MPC. The middle sub-figure shows the average temperature of the DHW tank in red, and temperature of each layer in blue.

4.3.3. Results for emission-oriented MPC controller

The emission-oriented MPC controller frequently charges the EV batteries right before departure to the required SOC level. EV_2, which is assumed to allow bidirectional charging, is frequently used as a temporary electrical storage, as Figs. 12 and 13 show. The same interruption of the yellow band occurs for the cost-oriented MPC controller.

4.3.4. Results for flexibility-oriented MPC controller

Results from the cost-oriented and emission-oriented MPC controllers motivate the design of the objective function in that maximizes flexibility availability. Results in Figs. 14 to 17 show that flexibility availability are consistent at low power levels can be sustained the longest. This prepares the building to be always ready to respond to a DSO's request to stay at low power levels, trading off reduced cost and emission saving as shown in Section 4.2.

A TES of 2 m^3 is further included and the results are summarized in Figs. 16 and 17. The SOC of the TES shows that the controller actively makes use of the thermal buffer. Due to this extra thermal storage, the yellow band is slightly wider than the case without TES as shown in Fig. 15, which means more power levels can be sustained for longer periods.

4.3.5. Comparison and discussion

The results show that the availability of flexibility is strongly correlated with power levels. First of all, most high power levels are only available for a short time because EVs are disconnected regularly, and the storage capacity of the batteries is limited. In addition, the high powers' available duration is strongly dependent on an EVs usage pattern since an unplugged EV is not available for flexibility provision. Low flexible power levels are sometimes only available for a few hours. This can be frequently observed for the cost-oriented controller in Fig. 11, for example. This is mainly the case because the EVs have to be charged quickly to a minimal SOC before departure due to a late start in charging. Last but not least, the control schemes have an impact on the availability of flexibility. Cost-oriented and emission-oriented MPC controllers tend to generate high-variance behaviors. With a flexibility-oriented MPC controllers, a more uniform and consistent distribution of availability is observed. This is especially true for low flexible power levels.

The described flexibility envelope can be communicated to the system operator periodically, as it is shown in Section 3. The operator can monitor the status of the grid in real-time and can send dispatch

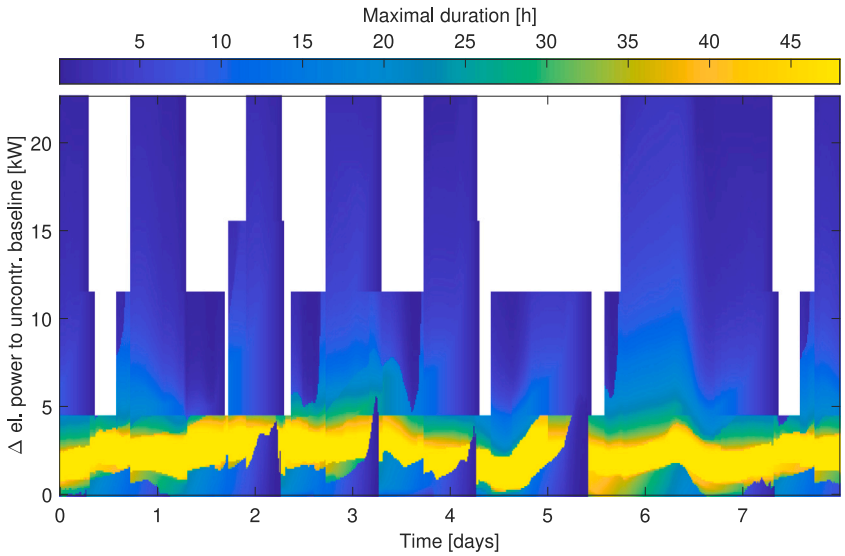

Fig. 11. Flexibility envelope of the building without TES operated by a cost-oriented MPC. The white area indicates infeasible power level at the specific times.

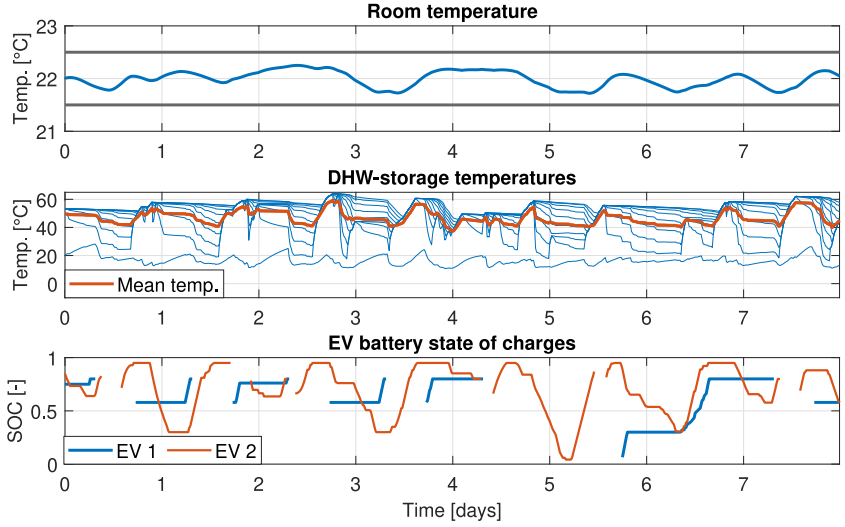

Fig. 12. States of the building without TES operated by a emission-oriented MPC. The middle sub-figure shows the average temperature of the DHW tank in red, and temperature of each layer in blue.

signals to the building energy management systems, such that they collectively adapt their energy schedules to alleviate network congestion, or address reverse flow by increasing local consumption. The required power levels can be conveniently achieved by stacking the powers of several buildings according to the identified flexibility envelope and corresponding operational limits. Since the envelope already takes into account the upcoming user's activities and boundary conditions, common concerns over rebound effects are reduced.

To further compare the flexibility levels across different cases, we define a total flexible time as the sum of the available duration of all flexible power levels. The total flexible time at time τ is defined as $Z_\tau = \sum_{P\in\mathbb{P}} f(\tau, P)$. Hence, the flexibility envelopes shown in Figs. 9, 11, 13, 15 and 17 can be further summarized and compared in the box plots shown in Fig. 18, which illustrates the distribution of Z_τ in all five cases. Flexibility of cost- and emission-oriented controllers have high variances and Z_τ approaches zero in extreme cases. In contrast, the flexibility-oriented controllers achieve higher means with lower variances, which implies a higher level of flexibility with lower uncertainty. In addition, TES further increases the mean value of Z_τ although variances remain similar.

5. Conclusion and outlook

There has been growing popularity in digitalizing electrical appliances in residential buildings and the installation of distributed renewable energy resources. It is critical to tap the flexibility of residential buildings and quantify it for further coordination at a system level, which would support agile and cost-efficient system operation. This study investigates the energy scheduling and flexibility quantification of electrical loads within one building and outlines a mechanism for using such flexibility at the system level.

We quantify flexibility by flexible power levels and determine the corresponding maximally sustainable duration. Simulation results show that the maximum flexible power level is strongly dependent on the availability of electric vehicles. The maximally sustained duration can be achieved for medium to low power levels, which approximately corresponds to the average upcoming load of all flexible electrical devices for the next 48 hours. In spring, heat pumps for space heating offer a long duration on low power levels. In contrast, the batteries of electric vehicles are flexible on a wide power range but for a shorter duration, which is mainly attributed to their daily usage pattern. For a building

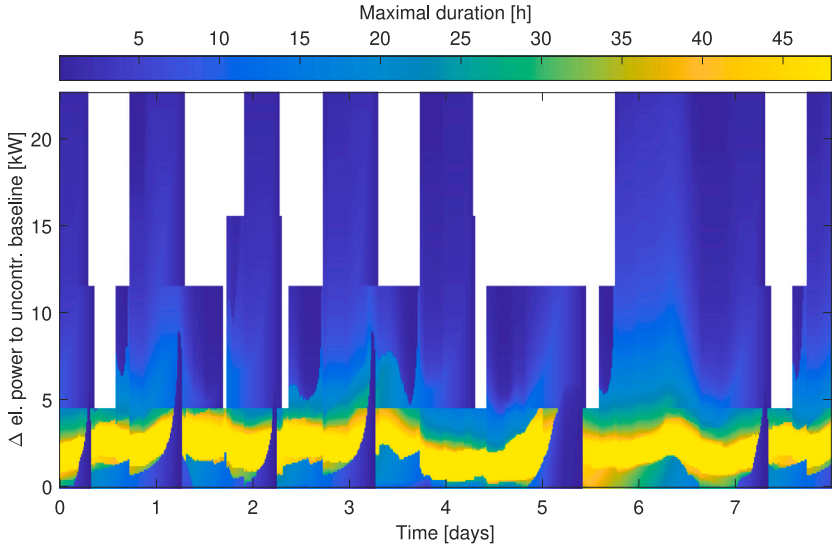

Fig. 13. Flexibility envelope of the building without TES operated by a emission-oriented MPC. The white area indicates infeasible power level at the specific times.

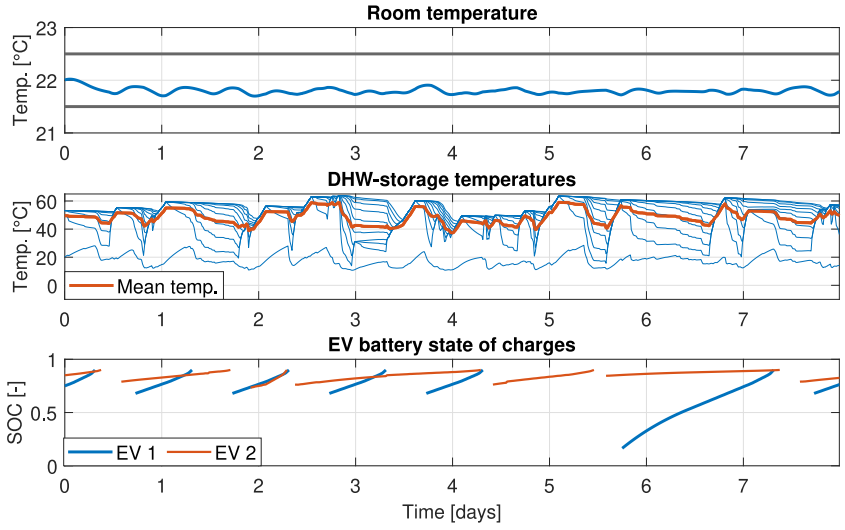

Fig. 14. States of the building without TES operated by a flexibility-oriented MPC.

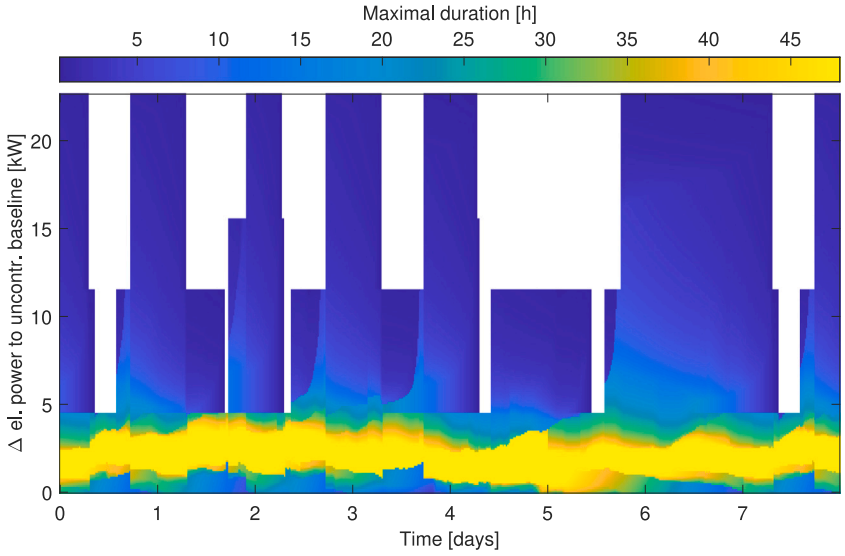

Fig. 15. Flexibility envelope of the building without TES operated by a flexibility-oriented MPC. The white area indicates infeasible power level at the specific times.

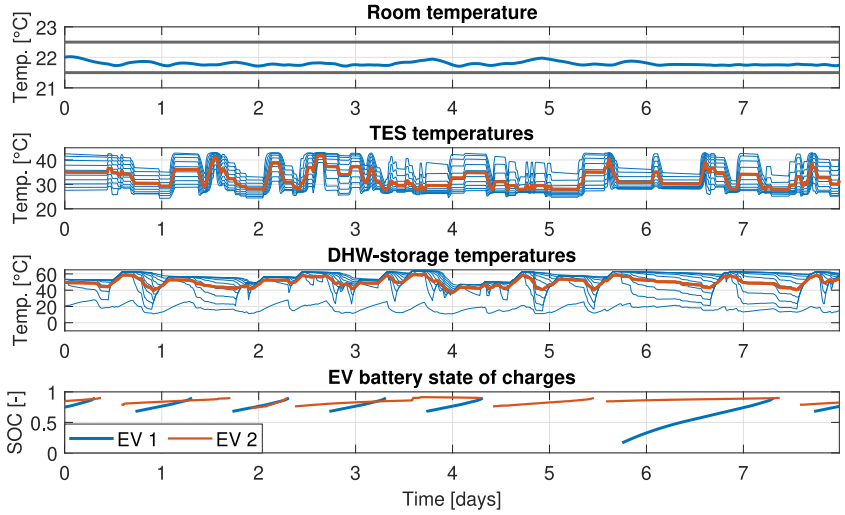

Fig. 16. States of the building with a TES of 2 m^3 operated by a flexibility-oriented MPC.

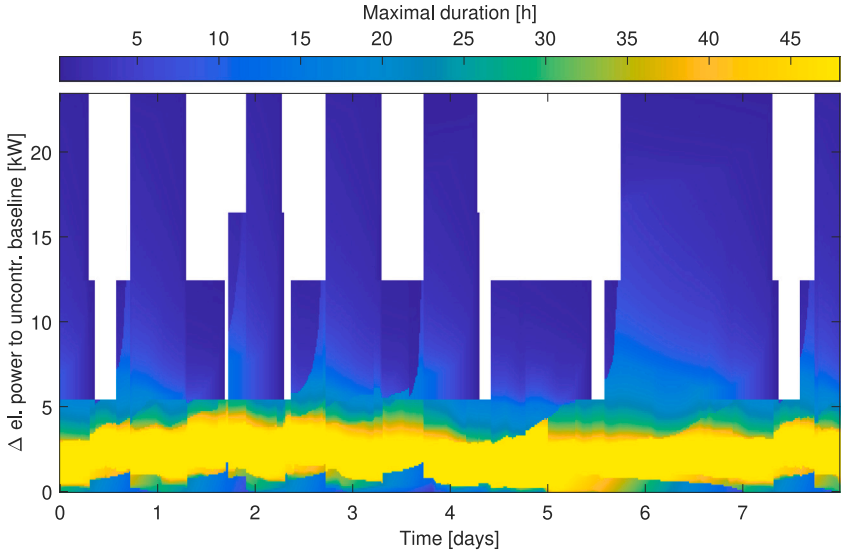

Fig. 17. Flexibility envelope of the building with a TES of 2 m^3 operated by a flexibility-oriented MPC. The white area indicates infeasible power level at the specific times.

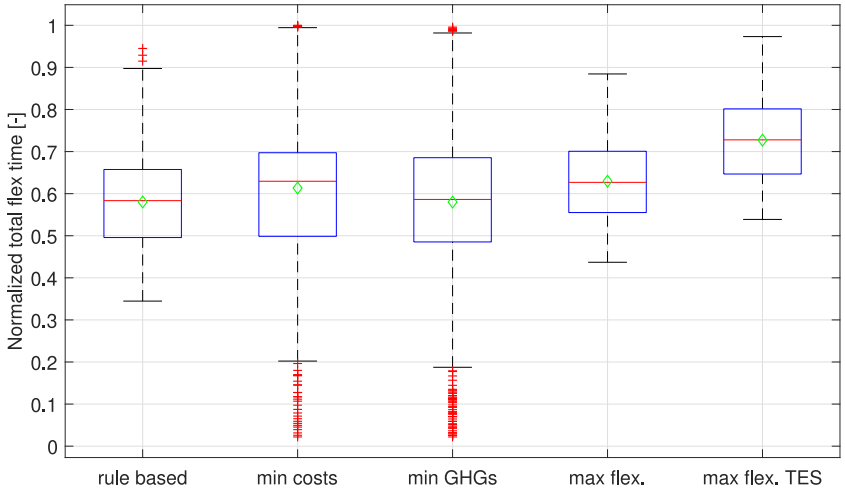

Fig. 18. Comparison of flexibility envelopes in all five cases using the total flexible time Z_t.

Table 5
Weekly driving profile of EV_1.

Day	Departure	Arrival	Driving distance [km]
Monday	07 : 30	17 : 30	60
Tuesday	07 : 30	17 : 30	60
Wednesday	07 : 30	17 : 30	60
Thursday	07 : 30	17 : 30	60
Friday	07 : 30	–	100
Saturday	–	18 : 00	100
Sunday	–	–	0

Table 6
Weekly driving profile of EV_2.

Day	Departure	Arrival	Driving distance [km]
Monday	09 : 00	14 : 00	20
Tuesday	17 : 00	22 : 00	30
Wednesday	07 : 00	09 : 00	25
Thursday	–	–	0
Friday	07 : 00	10 : 00	25
Saturday	11 : 00	14 : 00	10
Sunday	–	–	0

with thermal energy storage, a model predictive controller can achieve total cost savings of up to 25% compared to the rule-based controller. Optimal control aiming to minimize the carbon footprint shows that emissions can be reduced by up to 21%. We also propose buildings to be network-aware when constructing the flexibility envelope. Although the current study focuses on control and flexibility quantification at the building level, a framework to integrate flexibility into overall system management has also been outlined in the paper.

Nonetheless, there are several limitations of the current study. Firstly, only uni-directional charging is considered when computing flexibility envelopes. The envelope could be significantly enlarged by allowing bi-directional charging. Secondly, the flexibility quantification currently relies on sophisticated modeling and requires certain computational efforts for the identification. This might not be suitable for system operation with a higher temporal resolution. Future research will investigate a data-driven approach to alleviate the modeling and computational burdens. Lastly, perfect knowledge of boundary conditions is assumed. In practice, forecast errors are inevitable and the approach has to be adapted in a stochastic setting.

CRediT authorship contribution statement

Jan Gasser: Conceptualization, Methodology, Software, Validation, Formal analysis, Investigation, Writing - original draft, Writing - review & editing, Visualization. **Hanmin Cai:** Methodology, Formal analysis, Writing - original draft, Writing - review & editing, Visualization. **Stavros Karagiannopoulos:** Conceptualization, Methodology, Formal analysis, Writing - original draft, Writing - review & editing, Supervision. **Philipp Heer:** Conceptualization, Methodology, Formal analysis, Resources, Writing - review & editing, Supervision, Project administration. **Gabriela Hug:** Writing - review & editing, Supervision.

Declaration of competing interest

The authors declare that they have no known competing financial interests or personal relationships that could have appeared to influence the work reported in this paper.

Acknowledgment

This research project is financially supported by the Swiss Innovation Agency Innosuisse and is part of the Swiss Competence Center for Energy Research SCCER FEEB&D.

Appendix A. EV driving profiles

See Tables 5 and 6.

Table 7
PV-model parameters [23].

Parameter	Value	Unit
I_{peak}	4.65	[A]
U_{peak}	34.478	[V]
ΔI_{peak}	$2.42 \cdot 10^{-3}$	[–]
ΔU_{peak}	$-4.58 \cdot 10^{-3}$	[–]
K_1	−10.01	[V]
K_2	−1850.80	[V]
G_s	1000	[W/m^2]
T_s	298.15	[K]
T_{NOCT}	47	[°C]
A	1	[–]
q	$1.6 \cdot 10^{-19}$	[C]
k_b	$1.38 \cdot 10^{-23}$	[J/K]

Appendix B. PV model

The Photovoltaic (PV) model is adopted from [25] and [26]. The electrical power output of a panel is given as follows:

$$P_{PV}^{el} = I \cdot U \tag{12}$$

The current I and the voltage U are quantified according to the following equations:

$$I = I_{peak} \frac{G}{G_s} \left(1 + \Delta I_{peak}(T_{cell} - T_s)\right) \tag{13}$$

$$U = U_{peak}\left(1 + \Delta U_{peak}(T_{cell} - T_s)\right) + K_1 U_{th}\, ln\left(\frac{G}{G_s}\right) + K_2\left(U_{th}\, ln\left(\frac{G}{G_s}\right)\right)^2 \tag{14}$$

$$U_{th} = \frac{A\, k_b\, T_{cell}}{q} \tag{15}$$

$$T_{cell} = T_a + G(T_{NOCT} - 20) \tag{16}$$

where I_{peak} denotes the peak current, U_{peak} stands for the peak voltage, G_s is the standard solar radiation, T_{cell} is the module cell temperature, k_b denotes the Boltzmann constant, T_s is the standard temperature, T_a stands for the ambient temperature and T_{NOCT} is the normal operating cell temperatures. ΔI_{peak} and ΔU_{peak} are the temperature effects on the peak power current and on the peak power voltage respectively. K_1 and K_2 represent constant parameters. A and q represent the diode ideality factor and the charge of an electron respectively. The present normal radiation G is a function of the azimuth and tilt angle. The parameters are summarized in Table 7.

References

[1] Strbac G, Pudjianto D, Aunedi M, Djapic P, Teng F, Zhang X, Ameli H, Moreira R, Brandon N. Role and value of flexibility in facilitating cost-effective energy system decarbonisation. Prog Energy 2020.
[2] Liu Y, Bebic J, Kroposki B, De Bedout J, Ren W. Distribution system voltage performance analysis for high-penetration PV. In: 2008 IEEE energy 2030 conference. IEEE; 2008, p. 1–8.
[3] Hatta H, Uemura S, Kobayashi H, Engineering S. Cooperative control of distribution system with customer equipments to reduce reverse power flow from distributed generation. In: IEEE PES general meeting. IEEE; 2010, p. 1–6.
[4] Kathirgamanathan A, De Rosa M, Mangina E, Finn DP. Data-driven predictive control for unlocking building energy flexibility: A review. Renew Sustain Energy Rev 2021;135:110120.

[5] Taşcıkaraoğlu A, Paterakis NG, Erdinç O, Catalao JP. Combining the flexibility from shared energy storage systems and DLC-based demand response of HVAC units for distribution system operation enhancement. IEEE Trans Sustain Energy 2018;10(1):137–48.
[6] Olivella-Rosell P, Bullich-Massagué E, Aragüés-Peñalba M, Sumper A, Ottesen SØ, Vidal-Clos J-A, Villafáfila-Robles R. Optimization problem for meeting distribution system operator requests in local flexibility markets with distributed energy resources. Appl Energy 2018;210:881–95.
[7] Mathieu JL, Koch S, Callaway DS. State estimation and control of electric loads to manage real-time energy imbalance. IEEE Trans Power Syst 2012;28(1):430–40.
[8] Muthirayan D, Baeyens E, Chakraborty P, Poolla K, Khargonekar PP. A minimal incentive-based demand response program with self reported baseline mechanism. IEEE Trans Smart Grid 2019;11(3):2195–207.
[9] D'hulst R, Labeeuw W, Beusen B, Claessens S, Deconinck G, Vanthournout K. Demand response flexibility and flexibility potential of residential smart appliances: Experiences from large pilot test in Belgium. Appl Energy 2015;155:79–90.
[10] Golmohamadi H, Larsen KG, Jensen PG, Hasrat I. Optimization of power-to-heat flexibility for residential buildings in response to day-ahead electricity price. Energy Build 2020;110665.
[11] Leerbeck K, Bacher P, Junker RG, Tveit A, Corradi O, Madsen H. Control of heat pumps with CO2 emission intensity forecasts. Energies 2020;13(11):2851.
[12] Kathirgamanathan A, Péan T, Zhang K, De Rosa M, Salom J, Kummert M, Finn DP. Towards standardising market-independent indicators for quantifying energy flexibility in buildings. Energy Build 2020;110027.
[13] Finck C, Li R, Kramer R, Zeiler W. Quantifying demand flexibility of power-to-heat and thermal energy storage in the control of building heating systems. Appl Energy 2018;209:409–25.
[14] Heinrich C, Ziras C, Syrri AL, Bindner HW. Ecogrid 2.0: A large-scale field trial of a local flexibility market. Appl Energy 2020;261:114399.
[15] Chen X, Dall'Anese E, Zhao C, Li N. Aggregate power flexibility in unbalanced distribution systems. IEEE Trans Smart Grid 2020;11(1):258–69.
[16] Munankarmi P, Jin X, Ding F, Zhao C. Quantification of load flexibility in residential buildings using home energy management systems. In: Proceedings of the American control conference, vol. 2020-July. 2020, p. 1311–6.
[17] De Coninck R, Helsen L. Quantification of flexibility in buildings by cost curves–methodology and application. Appl Energy 2016;162:653–65.
[18] Federal Statistical Office and Swiss Federal Office of Energy. Energy - facts and figures. 2019, https://www.eda.admin.ch/aboutswitzerland/en/home/wirtschaft/energie/energie---fakten-und-zahlen.html, [Accessed: 6 April 2020].
[19] Federal statistical office Section Population. Heating system and energy sources. 2017, https://www.bfs.admin.ch/bfs/en/home/statistics/construction-housing/buildings/energy-field.html, [Accessed: 29 April 2020].
[20] Federal Statistical Office Section Mobility. Road vehicles - stock, level of motorisation. 2020, https://www.bfs.admin.ch/bfs/en/home/statistics/mobility-transport/transport-infrastructure-vehicles/vehicles/road-vehicles-stock-level-motorisation.html, [Accessed: 20 november 2020].
[21] Wimmer RW. Regelung einer Wärmepumpenanlage mit model predictive control. ETH Zurich; 2004.
[22] Verhelst C, Logist F, Van Impe J, Helsen L. Study of the optimal control problem formulation for modulating air-to-water heat pumps connected to a residential floor heating system. Energy Build 2012;45:43–53.
[23] Vrettos E, Lai K, Oldewurtel F, Andersson G. Predictive control of buildings for demand response with dynamic day-ahead and real-time prices. In: 2013 European control conference. IEEE; 2013, p. 2527–34.
[24] Karagiannopoulos S, Roald L, Aristidou P, Hug G. Operational planning of active distribution grids under uncertainty. In: Proceedings of the 10th bulk power systems dynamics and control symposium. 2017.
[25] Fakham H, Degobert P, Francois B. Control system and power management for a PV based generation unit including batteries. In: International aegean conference on electrical machines and power electronics. 2007, p. 141–6.
[26] Rauschenbach HS. Solar cell array design handbook - the principles and technology of photovoltaic energy conversion. 1980.
[27] Gasser J. Demand side flexibilities on a building level, a quantification of flexibility using thermal and electrical energy storages in combination with rule based and optimal control schemes. 2020, https://psl.ee.ethz.ch/Publications/SAMA.html, [Accessed: 02 january 2021].
[28] Zhang X, Schildbach G, Sturzenegger D, Morari M. Scenario-based MPC for energy-efficient building climate control under weather and occupancy uncertainty. In: 2013 European control conference. IEEE; 2013, p. 1029–34.
[29] werke die. Kundengruppe gewerbe mit leistungspreis; preise ab 1. Januar 2020. 2020, https://www.diewerke.ch/preislisten-strom, [Accessed: 06 april 2020].
[30] Löfberg J. YALMIP : A toolbox for modeling and optimization in MATLAB. In: Proceedings of the CACSD Conference. 2004.
[31] Gu Z, Rothberg E, Bixby R. GUROBI. 2020, https://support.gurobi.com, [Accessed: 18 march 2020].
[32] Empa. NEST Database. 2020, https://visualizer.nestcollaboration.ch, [Accessed: 17 march 2020].
[33] Pfenninger S, Staffell I. Long-term patterns of European PV output using 30 years of validated hourly reanalysis and satellite data. Energy 2016;114:1251–65.
[34] Beloin-Saint-Pierre D. Ecodynbat - ecobilan dynamique des Bâtiments. 2019, https://www.aramis.admin.ch/Grunddaten/?ProjectID=41804, [Accessed: 09 april 2020].